Symmetry breaking via hybridization with conduction electrons in frustrated Kondo lattices

Jeffrey G. Rau[1] and Hae-Young Kee[1,2,*]

[1]*Department of Physics, University of Toronto, Toronto, Ontario, Canada M5S 1A7*

[2]*Canadian Institute for Advanced Research/Quantum Materials Program, Toronto, Ontario, Canada MSG 1Z8*

(Received 26 June 2013; revised manuscript received 17 January 2014; published 21 February 2014)

In frustrated magnets when magnetic ordering is suppressed down to low temperature, the formation of a quantum spin liquid becomes a possibility. How such a spin liquid manifests in the presence of conduction electrons is a question with potentially rich physical consequences, particularly when both the localized spins and conduction electrons reside on frustrated lattices. We propose a mechanism for symmetry breaking in systems where conduction electrons hybridize with a quantum spin liquid through Kondo couplings. We apply this to the pyrochlore iridate $Pr_2Ir_2O_7$, which exhibits an anomalous Hall effect without clear indications of magnetic order. We show that hybridization between the localized Pr pseudospins and Ir conduction electrons breaks some of the spatial symmetries, in addition to time-reversal symmetry, regardless of the form of the coupling. These broken symmetries result in an anomalous Hall conductivity and induce small magnetic, quadrupolar, and charge orderings. Further experimental signatures are proposed.

DOI: 10.1103/PhysRevB.89.075128 PACS number(s): 75.10.Kt, 75.30.Mb, 75.70.Tj

I. INTRODUCTION

The study of interactions between itinerant electrons and localized degrees of freedom has led to an understanding of a wealth of novel physical phenomena. These range from isolated moments, as in the Kondo effect [1,2] through to the realm of dense lattices of moments as in heavy-fermion materials [3–5] and the anomalous Hall effect (AHE) [6]. While still largely unexplored, the interplay between itinerant degrees of freedom and frustrated local moments promises to unveil new and unique phases of matter [7]. One particularly interesting scenario arises when the local moments are highly frustrated, realizing a quantum spin liquid. How such a spin liquid competes with hybridization when conduction electrons are present has yet to be fully addressed [8–11].

In this article, we study systems where conduction electrons interact with a quantum spin liquid, introducing a mechanism for breaking spatial symmetries. When the conduction electrons hybridize with spinons the emergent gauge structure of the spin liquid is exposed. We show that a spin liquid with nontrivial gauge structure, i.e., fluxes penetrating the lattice, is incompatible with trivial gauge structure in the conduction states, breaking some of the spatial symmetries regardless of the details of hybridization. Such symmetry breaking has applications to Kondo lattice models where the high degree of frustration inhibits the appearance of magnetic order.

Specifically, we consider a model of conduction electrons and local moments on the pyrochlore lattice, where the effective fluxes are provided by choosing local quantization axes for the conduction electrons. While this is simply a basis choice when the electrons are isolated, when coupled with a fully symmetric U(1) spin liquid on the local moments any uniform hybridization forces the emergent magnetic flux through the plaquettes between the local moments and the conduction electrons [as shown in Fig. 1(b)], breaking some of the spatial symmetries.

To explore the consequences of such symmetry breaking, we consider $Pr_2Ir_2O_7$, where the praeseodymium (Pr) and iridium (Ir) atoms form a pair of interpenetrating pyrochlore lattices with space group $Fd\bar{3}m$, as shown in Fig. 1(a). The lack of indications of magnetic ordering [12] well below the Curie-Weiss temperature [13,14] suggests that the Pr sublattice is frustrated, either intrinsically or due to the presence of the Ir conduction electrons [15]. This is corroborated by features in the field-dependent magnetization at low temperatures, suggesting an antiferromagnetic interaction and possibly spin-ice physics, in contrast to the sign of the Curie-Weiss temperature [16]. In addition to these magnetic features, the compound is metallic [13], showing a finite AHE at intermediate temperatures between $\sim$0.3 and $\sim$1.5 K without evidence for a net magnetization to a resolution of $\sim 10^{-3}\mu_B$/Pr [16]. These unexplained properties have attracted considerable theoretical attention [16–21], along with a number of other unconventional features such as the lack of a clear phase transition into this intermediate phase as well as unusual behavior of the Hall conductivity in large fields [13,14,16], further enriching the problem.

The presence of an AHE along [111] requires a breaking of time-reversal symmetry and all of the spatial symmetries except for a C_3 symmetry along [111], inversion and a C_2 symmetry perpendicular to [111] followed by time reversal. Applying our idea to $Pr_2Ir_2O_7$, we find that hybridization between the Ir conduction electrons and a uniform U(1) quantum spin liquid on the Pr breaks the time-reversal and all of the spatial symmetries except a single C_3 axis and inversion, allowing an AHE. The orbital nature of this symmetry breaking provides a simple explanation for both the AHE and the smallness of the induced magnetic and quadrupolar moments.

II. CONDUCTION ELECTRONS

We first construct a minimal model for $Pr_2Ir_2O_7$, beginning with the Ir atoms. Assuming an ionic configuration of Ir^{4+} one has five d electrons per Ir. These Ir^{4+} ions form a pyrochlore lattice, face centered cubic with a tetrahedral basis,

*hykee@physics.utoronto.ca

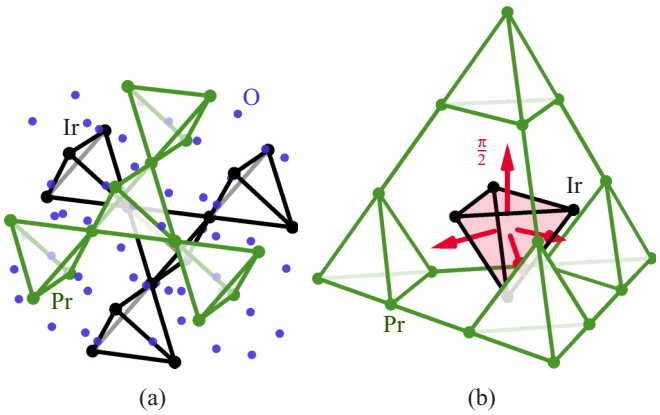

FIG. 1. (Color online) (a) Crystal structure of $Pr_2Ir_2O_7$. (b) Illustration of flux pattern induced from the local basis rotation, with spin-dependent parts ignored for clarity.

each surrounded by oxygens. The oxygens are approximately octahedrally coordinated about the Ir^{4+} ions, so we take the dominant crystal field environment to be O_h. The oxygen octahedra surrounding each Ir^{4+} ion in the unit cell are oriented differently, so the orbital mixing induced by the crystal fields is defined locally with respect to these octahedral axes. These crystal field effects are large, splitting the $5d$ levels into an e_g doublet and t_{2g} triplet. These are in a low-spin state so one can ignore the e_g doublet, considering a single hole in the t_{2g} states. Acting within the t_{2g} manifold, the orbital angular momentum behaves as $l_{\text{eff}} = 1$; spin-orbit coupling splits this into $j_{\text{eff}} = 1/2$ and $j_{\text{eff}} = 3/2$ states. Since the d orbitals are localized, the electronic structure of the Ir sublattice can be captured effectively using a tight-binding approach. If the spin-orbit coupling is sufficiently large compared with the bandwidth, the $j_{\text{eff}} = 3/2$ states can be discarded, and one can consider only a single half-filled $j_{\text{eff}} = 1/2$ band [22]. Working under these assumptions, the tight-binding parameters can be obtained by a symmetry construction or through explicit consideration of direct and oxygen-mediated hopping.

In the global cubic axes a symmetry operation S rotates the spin and orbital degrees of freedom according to some representation R_S. How these symmetry operations act with the local axes can be seen most clearly if we adopt quantization axes for the $j_{\text{eff}} = 1/2$ states that are compatible with the exact D_{3d} site symmetry of the Ir^{4+} ions. These axes are defined so that the $\hat{z}$ axis points along the local [111] direction and the $\hat{y}$ axis is oriented along one of the C_2' axes perpendicular to the local [111], with frames on different basis sites related by C_2 rotations. A symmetry operation S acts in this local basis as $U_{S(r)} R_S U_r^\dagger$ where U_r rotates the spin and orbital degrees of freedom into the local axes at site r. Projected into the $j_{\text{eff}} = 1/2$ levels, this simplifies to

$$P^\dagger U_{S(r)} R_S U_r^\dagger P = z_{S,r} L_S,$$

where $z_{S,r}$ is a sublattice-dependent sign and L_S is a local spin rotation. Explicit expressions for $z_{S,r}$ and L_S for each space group operation S are given in the Appendix.

Here we will work only with the nearest-neighbor hoppings, where aside from spin, the hopping matrices depend only on the four basis sites. Extension to further-neighbor hoppings is straightforward. Using symmetry operations in the local axes, $c_r^\dagger \to z_{S,r} L_S c_{S(r)}^\dagger$, one can show that there are only two allowed terms in the model:

$$H_{\text{Ir}} = \sum_{\langle rr' \rangle} i c_r^\dagger \left[t_1 \sigma^z \gamma_{rr'}^z + t_2 (\sigma^+ \gamma_{rr'}^+ + \sigma^- \bar{\gamma}_{rr'}^+) \right] c_{r'}, \quad (1)$$

where σ^μ are the Pauli matrices with $\sigma^\pm = (\sigma^x \pm i\sigma^y)/2$. The $\gamma_{rr'}^z$ and $\gamma_{rr'}^+$ depend only on the basis sites and can be written

$$\gamma^+ = \begin{pmatrix} 0 & +1 & +\bar{\omega} & +\omega \\ -1 & 0 & +\omega & -\bar{\omega} \\ -\bar{\omega} & -\omega & 0 & +1 \\ -\omega & +\bar{\omega} & -1 & 0 \end{pmatrix},$$

$$\gamma^z = \begin{pmatrix} 0 & +1 & +1 & +1 \\ -1 & 0 & +1 & -1 \\ -1 & -1 & 0 & +1 \\ -1 & +1 & -1 & 0 \end{pmatrix},$$

where $\omega = e^{2\pi i/3}$ and the functions $\gamma_{rr'}^z$ and $\gamma_{rr'}^+$ depend only on the pyrochlore sublattice indices, and $\bar{\gamma}_{rr'}^+$ denotes the complex conjugate of $\gamma_{rr'}^+$, and so can be written as the 4×4 matrices shown above. In this notation, the value of γ^z or γ^+ for a given r and r' can be found in the 4×4 matrix element whose row corresponds to the basis site in the unit cell of r and the column is the basis site of r'. Earlier studies used formal global axes for the $j_{\text{eff}} = 1/2$ bands [23,24], which can be obtained from the model derived above by transforming back into the global cubic axes using the U_r matrices.

III. NON-KRAMERS DOUBLETS AND PSEUDOSPINS

Having established a model for the Ir^{4+} ions, we now consider the Pr^{3+} ions. Since these states are highly localized, being in a $4f^2$ configuration, we use Hund's rules to arrive at the ground-state multiplet ${}^3H_4$, having quantum numbers $L = 5$, $S = 1$, and $J = 4$. The nine $J = 4$ states, denoted $|M\rangle$ with $|M| \leqslant 4$, are further split by crystal field effects, breaking into three E_g doublets and three singlets, two A_{1g} and one A_{2g}. Each is defined with respect to their local crystal axes. Due to the presence of a C_3 axis only states with $M - M' = 0 \pmod 3$ are mixed by the crystal field potential, breaking the multiplet into three sets: $|\pm 4\rangle, |\mp 2\rangle, |\pm 1\rangle$ and $|+3\rangle, |0\rangle, |-3\rangle$. Since two of the three-state sets are related by time-reversal symmetry they are degenerate, giving the three E_g representations. The remaining set mixes time-reversal partners and gives rise to the one-dimensional representations $2A_{1g}$ and A_{2g}. Inelastic neutron scattering studies of $Pr_2Ir_2O_7$ identify a ground-state doublet of E_g character, with the lowest-lying excited state a singlet at $\sim$162 K [25]. Since this scale is two orders of magnitude larger than the onset of the ordering, we can restrict consideration to only the ground-state doublet. Including the constraints from the remaining symmetries, this doublet has the form

$$|E_g, \pm\rangle = a_4 |\pm 4\rangle \pm a_1 |\pm 1\rangle - a_2 |\mp 2\rangle, \quad (2)$$

where a_4, a_2, and a_1 are real numbers depending on the details of the crystal field [26].

Within the space of doublets, superexchange interactions are mediated through the surrounding oxygen atoms. This can

be computed via a strong-coupling expansion, including the effects of hopping between the Pr $4f$ states and the O $2p$ states. When projected into the subspace of doublets, the exchange Hamiltonian is most convieniently written using pseudospin operators

$$\tau_r^\mu = \sum_{\alpha\beta} |E_g,\alpha\rangle_r \langle E_g,\beta|_r \sigma^\mu_{\alpha\beta}, \tag{3}$$

where $\alpha,\beta = \pm, \mu = x,y,z$ and $|E_g,\pm\rangle_r$ are the doublet states at site r. The τ_r^z operator is magnetic, proportional to the magnetic dipole moment, while the transverse τ_r^x and τ_r^y parts are nonmagnetic, carrying quadrupolar moments. All three exchanges allowed by symmetry are generated [27], giving the model in the local axes [26,28,29],

$$H_{\rm Pr} = \sum_{\langle rr'\rangle} \left[J_z \tau_r^z \tau_{r'}^z + \frac{J_\perp}{2}(\tau_r^+\tau_{r'}^- + \tau_r^-\tau_{r'}^+) \right] + J_{\pm\pm} \sum_{\langle rr'\rangle} (\gamma_{rr'}\tau_r^+\tau_{r'}^+ + \bar\gamma_{rr'}\tau_r^-\tau_{r'}^-), \tag{4}$$

and the sums run over nearest-neighbor bonds. Pseudospin rotational symmetry is not present when $J_z \neq J_\perp$ or in the presence of $J_{\pm\pm}$. The form of the $J_{\pm\pm}$ terms is a consequence of the intertwining of pseudospin and spatial symmetries, with the phases $\gamma_{rr'}$ defined as $\gamma_{rr'} = \bar\gamma^+_{rr'}\gamma^z_{rr'}$.

IV. HYBRIDIZATION

Let us consider interactions between the Pr and Ir sublattices, focusing on those mediated by hoppings between the sublattices, through physical or virtual processes. Charge transfer between the Pr and Ir necessarily involves intermediate states such as $4f^1$ or $4f^3$. For definiteness, we will assume that the $4f^1$ states are lower in energy than the $4f^3$ [26], and thus dominate, although our results do not depend fundamentally on this choice. In the D_{3d} crystal field this splits into a combination of Γ_{4u}, Γ_{5u}, and Γ_{6u} representations [30]. An example is the pair $\Gamma_{5u}+\Gamma_{6u}$, degenerate due to Kramers theorem, given by the $m = \pm 3/2$ states in the $j = 5/2$ manifold of the $4f^1$ configuration. Hybridization between the the $5d$ $j_{\rm eff} = 1/2$ states of the Ir and the localized states on the Pr can occur via several mechanisms, such as oxygen-mediated hoppings, but an effective description written as direct hopping is possible once the intermediate states have been integrated out. Considering only intermediate states Γ_{5u} and Γ_{6u}, the allowed hoppings are

$$H_{\rm hyb} = V_z \sum_{rr'} \gamma^z_{rr'} e^{i\pi\alpha/4} (-1)_{r,r'} c^\dagger_{r\alpha} |\Gamma_{5u}\rangle_{r'} \langle E_g,\bar\alpha|_{r'} + V_\pm \sum_{rr'} \gamma^\alpha_{rr'} e^{i\pi\alpha/4} (-1)_{r,r'} c^\dagger_{r\alpha} |\Gamma_{5u}\rangle_{r'} \langle E_g,\bar\alpha|_{r'} + \text{time reversed} + \text{H.c.},$$

where $\bar\alpha = -\alpha$, r is an Ir site, r' is a Pr site, and $\gamma^-_{rr'} = \bar\gamma^+_{rr'}$. If one splits the Ir-Pr bonds into two sets, related by inversion, then $(-1)_{r,r'}$ is $+1$ on the first set and -1 on the second. This pattern is shown for the Pr-centered hexagons in Fig. 2. To derive this form, one must keep in mind that the Γ_{5u} and Γ_{6u} states are Kramers states and defined in the local axes, and so carry the same signs $z_{S,r}$ as the $j_{\rm eff} = 1/2$ states in their symmetry operations. For simplicity we set $V_\pm = 0$ for the remainder of this work, as it does not affect the results qualitatively.

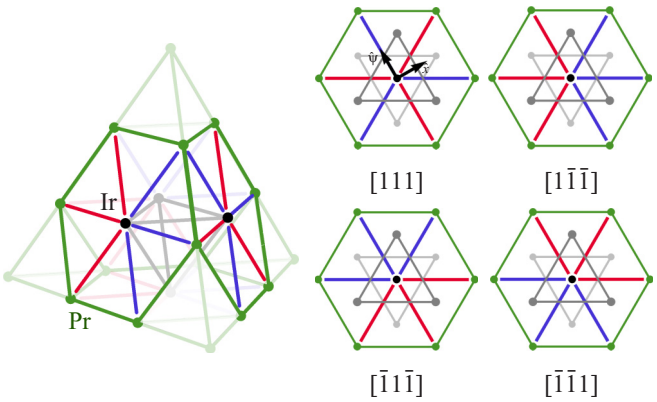

FIG. 2. (Color online) Hybridization form factor $(-1)_{r,r'}\gamma^z_{rr'}$ for Γ_{5u} and Γ_{6u} intermediate states, where $+1$ is shown in blue and -1 in red. Explicit form factors for the hexagon in each [111] plane are shown alongside, oriented so that the local $\hat x$ axis at the central site is 60° from the vertical.

We consider a fermionic slave-particle approach, as this allows for a natural treatment of hybridization between the Pr and Ir. The transition operators $|\Gamma_{5u}\rangle_r\langle E_g,\alpha|_r$ and $|\Gamma_{6u}\rangle_r\langle E_g,\alpha|_r$ are written using a pseudospinon $\eta_{r\alpha}$ and auxiliary bosons Φ_5 and Φ_6,

$$|\Gamma_{5u}\rangle_r\langle E_g,\alpha|_r = \Phi^\dagger_{5,r}\eta_{r\alpha}, \tag{5}$$

$$|\Gamma_{6u}\rangle_r\langle E_g,\alpha|_r = \Phi^\dagger_{6,r}\eta_{r\alpha}. \tag{6}$$

These slave particles are constrained to satisfy $\eta^\dagger_r\eta_r + \Phi^\dagger_{5,r}\Phi_{5,r} + \Phi^\dagger_{6,r}\Phi_{6,r} = 1$. Since these pseudospinons are of non-Kramers character, the symmetry operations in this local basis do not carry the signs $z_{S,r}$ and transform simply as $\eta^\dagger_r \to M_S\eta^\dagger_r$ where M_S is the pseudospin rotation corresponding to the symmetry operation S. The Φ_5 and Φ_6 bosons transform as the associated one-dimensional representations, but being Kramers states in the local quantization axes they also carry the phase factors $z_{S,r}$ and transform as $\Phi_{5,r} \to z_{S,r}e^{i\phi_{5,S}}\Phi_{5,S(r)}$ and $\Phi_{6,r} \to z_{S,r}e^{i\phi_{6,S}}\Phi_{6,S(r)}$ under the symmetry operation S.

When splitting Δ between the E_g and the excited states is large we expect condensation of the bosons $\Phi_{5,r}$ and $\Phi_{6,r}$ at order Δ^{-1}. In this limit the constraint can be simplified to $\eta^\dagger_r\eta_r \sim 1$. With the condensation only in the Φ_5 channel, one has an effective hopping between electron $c^\dagger_r$ and spinon $\eta_{r'}$,

$$H_{\rm hyb} \sim V \sum_{rr'} \gamma^z_{rr'} e^{i\pi\alpha/4} (-1)_{r,r'} c^\dagger_{r\alpha}\eta_{r'\bar\alpha} + \text{H.c.}, \tag{7}$$

where we have absorbed Φ^*_5 into V_z, defining $V \equiv V_z\Phi^*_5$. Condensing in either the Φ_5 or Φ_6 channel breaks time-reversal symmetry and time-reversal symmetry squared, similarly to the hastatic order proposed for URu_2Si_2 [31]. However the one-dimensional nature of Γ_{5u} and Γ_{6u} allows the combination $H_{\rm Ir} + H_{\rm hyb}$ to break none of the spatial symmetries of the

problem, a key difference from the case considered in Ref. [31].

V. NON-KRAMERS SPIN LIQUIDS

The exchange interactions between the Pr pseudospins will induce interactions between the pseudospinons η_r. In terms of the slave particles the pseudospin operator is given by $\tau_r^\mu = \frac{1}{2}\eta_r^\dagger \sigma^\mu \eta_r$. To render the problem tractable, we consider an approximate ground state generated from a Hamiltonian quadratic in the fermions. Variational Monte Carlo calculations [32,33] on the Heisenberg model motivate us to consider two classes of U(1) spin-liquid *Ansätze*, the uniform and monopole states which are competitive in this limit. The monopole *Ansatz* is a chiral spin liquid, breaking time-reversal and inversion symmetry but preserving the product, and can be characterized by hoppings carrying a flux of $\pi/2$ exiting the faces of each tetrahedron. The uniform state has equal hoppings on all bonds, carrying zero flux through all plaquettes. Since the presence of $J_{\pm\pm}$ or $J_z \neq J_\perp$ breaks SU(2) pseudospin rotational symmetry, these *Ansätze* must be extended using their respective projective symmetry group (PSG) [34] to include pseudospin-dependent $E^\alpha_{rr'}$ hoppings in addition to the pseudospin-independent $\chi_{rr'}$ hoppings allowed at the SU(2) symmetric point. Each spin-liquid *Ansatz* is characterized by a quadratic Hamiltonian

$$H(\chi, E) = \sum_{\langle rr' \rangle} \left(\chi_{rr'} \eta_r^\dagger \eta_{r'} + \sum_\alpha E^\alpha_{rr'} \eta_r^\dagger \sigma^\alpha \eta_{r'} \right),$$

where the single-occupancy constraint is implemented on average through chemical potentials λ_r tuned to enforce $\langle \eta_r^\dagger \eta_r \rangle = 1$. To gain insight into which spin liquid may be favored as we move away from the Heisenberg limit, for each *Ansatz* Hamiltonian $H(\chi, E)$ we compute the ground state $|\psi(\chi, E)\rangle$. The energy $\epsilon(\chi, E) = \langle \psi(\chi, E)|H_{\rm Pr}|\psi(\chi, E)\rangle$, where $H_{\rm Pr}$ is the full Pr Hamiltonian, is then minimized with respect to χ and E. The phase diagram is shown in Fig. 3(b), giving the state with lowest ϵ as a function of $J_\perp/J_z$ and $J_{\pm\pm}/J_z$.

The monopole *Ansatz* occupies a large region of the phase diagram around the Heisenberg point, and has two triplet terms E^z_m and E^+_m. The E^+_m terms have the values $E^+_{ab} = iE^+_m \bar{\gamma}^+_{ab}$ for bonds within the unit cell and $-iE^+_m \bar{\gamma}^+_{ab}$ for bonds that leave the unit cell, and the E^z_m terms are of the form $E^z_{ab} = iE^z_m \gamma^z_{ab}$. The E^z_m becomes relevant when $J_z \neq J_\perp$ and $J_{\pm\pm} \neq 0$, while

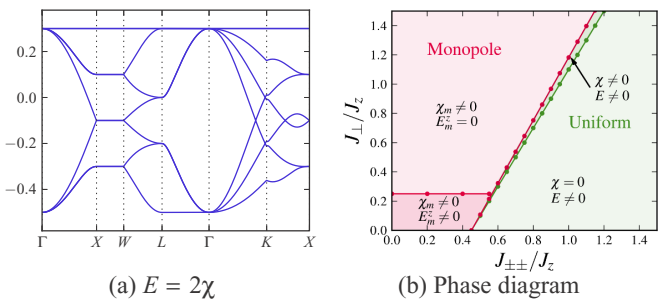

(a) $E = 2\chi$ (b) Phase diagram

FIG. 3. (Color online) (a) The band structure of the uniform *Ansatz* for $E = 2\chi = 0.1$. (b) The phase diagram considering triplet extensions to both the monopole and uniform *Ansätze*.

the E^+_m term is disfavored throughout the phase diagram as shown in Fig. 3(b). The uniform state is favored when $J_{\pm\pm}$ is of order $\sim J_z/2$ as shown in Fig. 3(b) This *Ansatz* is fully symmetric with trivial PSG, having the simple form $\chi_{rr'} = \chi$, $E^+_{rr'} = \bar{\gamma}_{rr'} E$, and $E^z_{rr'} = 0$. We show the dispersion of this state when $E \neq 0$ and $\chi = E/2$ in Fig. 3(a). Note the lack of doubly degenerate bands, despite the presence of both time-reversal and inversion symmetry, due to these pseudospinons being non-Kramers states. We can understand the dominance of the uniform phase in the limit $J_{\pm\pm} \gg J_z, J_\perp$. There we expect the $E^x_{rr'}$ and $E^y_{rr'}$ terms to dominate, and the selection of this phase can be understood from the mean-field quadratic terms

$$\langle H_{\rm Pr} \rangle \sim -\frac{J_{\pm\pm}}{2} \begin{pmatrix} \bar{E}^x_{rr'} & \bar{E}^y_{rr'} \end{pmatrix} \begin{pmatrix} \cos\phi_{rr'} & -\sin\phi_{rr'} \\ -\sin\phi_{rr'} & -\cos\phi_{rr'} \end{pmatrix} \begin{pmatrix} E^x_{rr'} \\ E^y_{rr'} \end{pmatrix}. \tag{8}$$

The eigenvector of this matrix with largest negative eigenvalue is given by

$$\begin{pmatrix} E^x_{rr'} \\ E^y_{rr'} \end{pmatrix} \propto \begin{pmatrix} 1 \\ 0 \end{pmatrix}, \quad \begin{pmatrix} -\frac{1}{2} \\ +\frac{\sqrt{3}}{2} \end{pmatrix}, \quad \begin{pmatrix} -\frac{1}{2} \\ -\frac{\sqrt{3}}{2} \end{pmatrix} \tag{9}$$

for $\phi_{rr'} = 0, +\frac{2\pi}{3}$, and $-\frac{2\pi}{3}$, respectively, the same form as in the uniform *Ansatz*. This also provides an explanation for the absence of the E^+_m term when $J_{\pm\pm} \neq 0$.

VI. BROKEN SYMMETRIES

We now consider the full Hamiltonian $H = H_{\rm Ir} + H_{\rm hyb} + H_{\rm Pr}$, including a uniform U(1) spin liquid on the Pr. When the Φ_5 boson condenses the U(1) × U(1) gauge symmetry of the decoupled electron and spin-liquid system is broken to a single U(1) symmetry [8,35], given by the transformation $\eta \to e^{i\theta}\eta$ and $c \to e^{i\theta}c$. This breaking of the relative gauge symmetry results in a Meissner-like effect, with a mass term pinning the emergent and physical gauge fields together. This pinning manifests itself in the acquisition of electric charge by the pseudospinon η, allowing the η pseudospinons to contribute directly to the Fermi sea as well as electromagnetic properties of the system [36]. A more general problem, which can be accessed by considering further intermediate $4f^1$ and $4f^3$ channels, is an arbitrary hybridization

$$H_{\rm hyb} \sim \sum_{rr'} \sum_{\alpha\beta} V^{\alpha\beta}_{rr'} c^\dagger_{r\alpha} \eta_{r'\beta} + \text{H.c.} \tag{10}$$

Any choice of this $V_{rr'}$, when both $H_{\rm Ir}$ and $H_{\rm Pr}$ are present, will result in not only a breaking of time-reversal but in addition a breaking of at least one of the spatial symmetries. This is due to an incompatibility between the gauge structures of the Ir and Pr sublattices. For all operations S in $Fd\bar{3}m$, a symmetric hybridization must have

$$V_{rr'} = z_{S,r} e^{i\theta_S} L_S V_{S^{-1}(r),S^{-1}(r')} M_S^\dagger \tag{11}$$

for some choice of phases $e^{i\theta_S}$. Since the symmetries in the local axes form a group, for any operations S and S' the action of SS' must be equivalent to the action of S' followed by S. The local rotations satisfy $L_{SS'} = L_S L_{S'}$, so an equation relating

$z_{SS',r}$ to $z_{S,r}$ and $z_{S',r}$ can be obtained. Explicitly, this is given by [34]

$$z_{SS',r} = \eta_{S,S'} z_{S,r} z_{S',S^{-1}(r)} \tag{12}$$

with $\eta_{S,S'} = \pm 1$. When combined with Eq. (11) this consistency condition entails that $\eta_{S,S'}$ be gauge equivalent to 1. For the $z_{S,r}$ this is false, and so this is satisfied only by some subgroup of $Fd\bar{3}m$, breaking some of the symmetry.

The specific form shown in Eq. (7), motivated by the Anderson limit, breaks all spatial symmetries except for inversion and a single C_3 axis. In the gauge used throughout the paper this is the [111] axis. As shown in Fig. 1(b), if spin dependence is ignored, then we can understand the gauge structure in a qualitative fashion as a flux of $\pi/2$ exiting each tetrahedral face of the Ir sublattice. With the uniform spin liquid on the Pr and $V_{rr'}$ on the Pr-Ir bonds chosen as in Eq. (7), the flux is trapped in this truncated tetrahedron. Since the flux is not exiting, it must recombine into 2π flux somewhere within the volume. We have arranged it to preserve one of the C_3 axes. When the Pr bonds are not present, this flux can cancel inside the remaining tetrahedra and thus form a symmetric state. In the presence of Pr-Ir bonds, a flux passes through the plaquettes between the Pr and Ir, breaking the symmetries. Since the only remaining symmetries are inversion and a single C_3 axis symmetry, the system is sufficiently asymmetric such that the AHE is allowed along the [111] direction. Further magnetic, charge, and quadrupolar orderings are generically induced, subject only to this fairly permissive C_3 symmetry and inversion.

VII. DISCUSSION

To explore the effects of the spin-liquid parameters and hybridization we fix $t_1 = 1$, $t_2 = 0.1t_1$, and $\chi = E/2$ and vary E and V, where χ and E are spin-independent and spin-dependent hopping terms. This assumes that $J_{\pm\pm}/J_z$ is sufficiently large so that a uniform spin liquid is stabilized. Calculations of AHE coefficients and magnetization are shown in Figs. 4(a) and 4(b). The magnetization shows the net magnetic moment per Pr atom, oriented along the [111], with contributions from both Pr and Ir sublattices [as shown in Figs. 4(c) and 4(d)] using g factors of $g_{\mathrm{Pr}} \sim 6.0$ and $g_{\mathrm{Ir}} \sim 2.0$. The anomalous Hall vector $\vec{\sigma}_A$ is computed using the Kubo formula [6], where the pseudospinons contribute as electrons to the current operators in the condensed phase.

The large AHE with small magnetic moments is in qualitative agreement with the properties of the intermediate phase of $Pr_2Ir_2O_7$. Here both the AHE and magnetic moment are larger than observed experimentally, except at small values of V. This discrepancy can be explained if the domains of the ordered phase are not fully aligned by the hysteresis process; then the observed AHE and magnetization would represent residual contributions from the partially aligned domains. At the mean-field level one expects that the transition into the hybridized phase should show a jump in the specific heat. Since the order parameter can take eight directions along the [111] axes one expects the critical theory to be described by an O(3)-type model, leading to a cusp at the transition. The effects of disorder or Pr-Ir substitution can potentially smooth this cusp into the broad peak seen in experiments [16] once

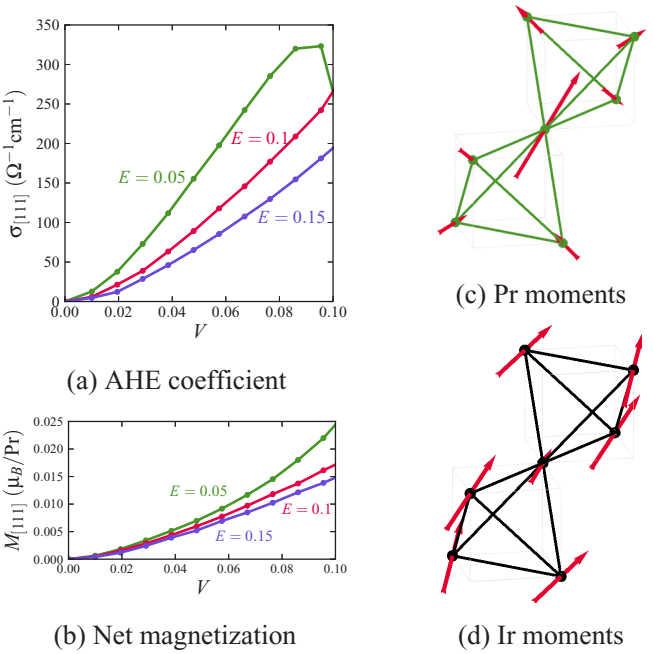

FIG. 4. (Color online) The AHE coefficient (a) and net magnetization (b) along the [111] direction for several values of E as functions of V, with t_2/t_1 fixed at 0.1 and $\chi/E = 0.5$. The pattern of local magnetic and quadrupolar moments on the Pr (c) and of local magnetic moments on the Ir (d).

background contributions have been subtracted. The onset of hybridization between the pseudospinons and the electrons alters the electronic band structure. How this manifests itself at the transition depends on the gauge fluctuations, as the binding of electric charge to the pseudospinons softens as one approaches the critical point.

An essential feature of our proposal is the lack of large on-site moments. All induced orderings, such as the magnetic, quadrupolar, and charge modulations, are small, appearing only at fractions $\sim 10^{-2}$–10^{-3} of their saturated values. This is distinct from scenarios with large moments [16,21] on the Pr and Ir sites, but that approximately cancel leaving a small net moment at the oxygen site. To distinguish these experimentally, nuclear magnetic resonance (NMR) on the oxygens is promising. In the crystal structure the oxygens lie in two inequivalent Wyckoff positions: the 8a position, which has tetrahedral symmetry and the 48f position which is in an asymmetric location. If one can account for the small net moment through a cancellation of large local moments, then one may expect the net field at the symmetric site 8a to be small, but generically the asymmetric site 48f should be affected by a net field from moments of order $\sim \mu_B$. Assuming dipolar fields from the moments acting at the oxygen sites, one then expects the effect at the 48f site to be several orders of magnitude larger than that of the 8a site. Our proposal predicts a significantly different result, with the small local moments producing only small fields of order $\sim$0.1–1 G at both oxygen sites.

In conclusion, we have proposed a mechanism for symmetry breaking when conduction electrons hybridize with a quantum spin liquid. This mechanism could potentially be manifested in a wide range of heavy-fermion materials on geometrically frustrated lattices. Applied to $Pr_2Ir_2O_7$,

we found that the hybridization of two subsystems (f and d electrons) results in a chiral nematic metal with broken time-reversal and spatial symmetries, exhibiting an anomalous Hall effect without a sizable magnetic moment.

ACKNOWLEDGMENTS

We would like to thank S. B. Lee, Y. B. Kim, L. Balents, S. Bhattacharjee, and A. Paramekanti for helpful discussions. This work was supported by the NSERC of Canada.

APPENDIX A: LOCAL AXES AND SYMMETRIES

We consider a basis for a pyrochlore lattice where the sites b_a are given by

$$b_1 = \frac{1}{8}\begin{pmatrix}+1\\+1\\+1\end{pmatrix}, \quad b_2 = \frac{1}{8}\begin{pmatrix}-1\\+1\\+1\end{pmatrix}, \quad b_3 = \frac{1}{8}\begin{pmatrix}+1\\-1\\+1\end{pmatrix}, \quad b_4 = \frac{1}{8}\begin{pmatrix}+1\\+1\\-1\end{pmatrix}. \tag{A1}$$

For each of these four sites we define local axes

$$\hat{z}_1 = \frac{1}{\sqrt{3}}\begin{pmatrix}+1\\+1\\+1\end{pmatrix}, \quad \hat{z}_2 = \frac{1}{\sqrt{3}}\begin{pmatrix}-1\\+1\\+1\end{pmatrix}, \quad \hat{z}_3 = \frac{1}{\sqrt{3}}\begin{pmatrix}+1\\-1\\+1\end{pmatrix}, \quad \hat{z}_4 = \frac{1}{\sqrt{3}}\begin{pmatrix}+1\\+1\\-1\end{pmatrix},$$
$$\hat{x}_1 = \frac{1}{\sqrt{6}}\begin{pmatrix}-2\\+1\\+1\end{pmatrix}, \quad \hat{x}_2 = \frac{1}{\sqrt{6}}\begin{pmatrix}-2\\-1\\-1\end{pmatrix}, \quad \hat{x}_3 = \frac{1}{\sqrt{6}}\begin{pmatrix}+2\\+1\\-1\end{pmatrix}, \quad \hat{x}_4 = \frac{1}{\sqrt{6}}\begin{pmatrix}+2\\-1\\+1\end{pmatrix}, \tag{A2}$$

where the remaining axis is given by $\hat{y}_a = \hat{z}_a \times \hat{x}_a$. We define rotations of the d levels U_r at each site r that take the global cubic axes to the local frames. To understand how symmetries act within this basis we first must consider the global axes, where a symmetry S acts on the spin and orbital degrees of freedom of the d levels via some matrix R_S. Then it is clear that the symmetry S acts in the local frame as $U_{S(r)} R_S U_r^\dagger$. This set of quantization axes for the pyrochlore lattice has the advantage of acting only in the local frames, with the rotations of the local spin being the same across all the basis sites of the lattice up to a sign. Explicitly, one finds

$$P^\dagger U_{S(r)} R_S U_r^\dagger P = z_{S,r} L_S, \tag{A3}$$

where the operator P projects into the $j_{\text{eff}} = 1/2$ subspace of the d levels. The $z_{S,r}$ is a sign that depends only on the basis site of the pyrochlore lattice. The rotations L_S can be found using the information in Table I, by mapping each of the group elements to the appropriate Γ_{4g} operation for the $j_{\text{eff}} = 1/2$ levels. Up to an unimportant overall sign this corresponds to mapping to SU(2) rotations. For example, to find the local rotation L_S where S is a C_2 rotation about the [110] axis (for our purpose we can ignore the translational part), we take the $6C_2'$ row and [110] column in Table I, which shows that the D_{3d} operation is $C_3^{-1} C_2 C_3$. We then construct the SU(2) rotations for these elements (the Γ_{4g} representation), which has $C_2 \to i\sigma_y$ and $C_3 \to e^{-i\pi\sigma_z/3}$. Finally putting these together we have that $L_{C_2,[110]} = i\sigma_y e^{-2\pi i \sigma_z/3}$.

The gauge transformations can be found in Table II and in Ref. [33]. The signs depend only on the sublattice so we write $z_{S,r} \equiv z_{S,a}$ where $a = 1,2,3,4$. We give here only the gauge transformations for the proper rotations, as the improper elements (those with an inversion) have the same sign structure. The gauge transformation for the inverse of a given element can also be easily computed.

TABLE I. The mapping of the space group operations of $Fd\bar{3}m$ into operations D_{3d} in the local basis. We organize these by conjugacy class, showing the operation L_S for each element indexed by the rotation axis. The elements $1, C_2, C_3$ denote the proper rotations of D_{3d} while I, σ_d, S_6 are the corresponding improper elements.

Class	Axis							
$8C_3$	[111]	$[1\bar{1}\bar{1}]$	$[\bar{1}1\bar{1}]$	$[\bar{1}\bar{1}1]$	$[\bar{1}\bar{1}\bar{1}]$	$[\bar{1}11]$	$[1\bar{1}1]$	$[11\bar{1}]$
	C_3	C_3	C_3	C_3	C_3^{-1}	C_3^{-1}	C_3^{-1}	C_3^{-1}
$6C_4$	[100]	[010]	[001]	$[\bar{1}00]$	$[0\bar{1}0]$	$[00\bar{1}]$		
	C_2	$C_3C_2C_3^{-1}$	$C_3^{-1}C_2C_3$	C_2	$C_3C_2C_3^{-1}$	$C_3^{-1}C_2C_3$		
$3C_2$	[100]	[010]	[001]					
	1	1	1					
$6C_2'$	[011]	$[01\bar{1}]$	[101]	$[10\bar{1}]$	[110]	$[1\bar{1}0]$		
	C_2	C_2	$C_3C_2C_3^{-1}$	$C_3C_2C_3^{-1}$	$C_3^{-1}C_2C_3$	$C_3^{-1}C_2C_3$		
$8IC_3$	[111]	$[1\bar{1}\bar{1}]$	$[\bar{1}1\bar{1}]$	$[\bar{1}\bar{1}1]$	$[\bar{1}\bar{1}\bar{1}]$	$[\bar{1}11]$	$[1\bar{1}1]$	$[11\bar{1}]$
	S_6	S_6	S_6	S_6	S_6^{-1}	S_6^{-1}	S_6^{-1}	S_6^{-1}
$6IC_4$	[100]	[010]	[001]	$[\bar{1}00]$	$[0\bar{1}0]$	$[00\bar{1}]$		
	σ_d	$C_3\sigma_dC_3^{-1}$	$C_3^{-1}\sigma_dC_3$	σ_d	$C_3\sigma_dC_3^{-1}$	$C_3^{-1}\sigma_dC_3$		
$3IC_2$	[100]	[010]	[001]					
	I	I	I					
$6IC_2'$	[011]	$[01\bar{1}]$	[101]	$[10\bar{1}]$	[110]	$[1\bar{1}0]$		
	σ_d	σ_d	$C_3\sigma_dC_3^{-1}$	$C_3\sigma_dC_3^{-1}$	$C_3^{-1}\sigma_dC_3$	$C_3^{-1}\sigma_dC_3$		

TABLE II. The $z_{S,r}$ signs required to implement symmetries in the local axes. The gauge has been chosen so that $z_{S,1} = 1$ for all of the symmetries S.

C_3	$z_{C_3,1}$	$z_{C_3,2}$	$z_{C_3,3}$	$z_{C_3,4}$	C_4	$z_{C_4,1}$	$z_{C_4,2}$	$z_{C_4,3}$	$z_{C_4,4}$
[111]	+1	+1	+1	+1	[100]	+1	−1	+1	+1
$[1\bar{1}\bar{1}]$	+1	+1	−1	−1	[010]	+1	+1	−1	+1
$[\bar{1}1\bar{1}]$	+1	−1	+1	−1	[001]	+1	+1	+1	−1
$[\bar{1}\bar{1}1]$	+1	−1	−1	+1					
C_2'	$z_{C_2',1}$	$z_{C_2',2}$	$z_{C_2',3}$	$z_{C_2',4}$	C_2	$z_{C_2,1}$	$z_{C_2,2}$	$z_{C_2,3}$	$z_{C_2,4}$
[011]	+1	+1	−1	+1	[100]	+1	−1	−1	+1
$[01\bar{1}]$	+1	−1	−1	−1	[010]	+1	+1	−1	−1
[101]	+1	+1	+1	−1	[001]	+1	−1	−1	−1
$[10\bar{1}]$	+1	−1	−1	−1					
[110]	+1	−1	+1	+1					
$[1\bar{1}0]$	+1	−1	−1	−1					

[1] J. Kondo, Prog. Theor. Phys. **32**, 37 (1964).
[2] K. G. Wilson, Rev. Mod. Phys. **47**, 773 (1975).
[3] G. Stewart, Rev. Mod. Phys. **56**, 755 (1984).
[4] S. Doniach, Physica B+C **91**, 231 (1977).
[5] A. C. Hewson, *The Kondo Problem to Heavy Fermions* (Cambridge University Press, Cambridge, 1997), Vol. 2.
[6] N. Nagaosa, J. Sinova, S. Onoda, A. MacDonald, and N. Ong, Rev. Mod. Phys. **82**, 1539 (2010).
[7] Q. Si, Physica B **378**, 23 (2006).
[8] T. Senthil, S. Sachdev, and M. Vojta, Phys. Rev. Lett. **90**, 216403 (2003).
[9] T. Senthil, M. Vojta, and S. Sachdev, Phys. Rev. B **69**, 035111 (2004).
[10] P. Ghaemi and T. Senthil, Phys. Rev. B **75**, 144412 (2007).
[11] P. Coleman and A. H. Nevidomskyy, J. Low Temp. Phys. **161**, 182 (2010).
[12] D. MacLaughlin, Y. Ohta, Y. Machida, S. Nakatsuji, G. Luke, K. Ishida, R. Heffner, L. Shu, and O. Bernal, Physica B **404**, 667 (2009).
[13] S. Nakatsuji, Y. Machida, Y. Maeno, T. Tayama, T. Sakakibara, J. van Duijn, L. Balicas, J. N. Millican, R. T. Macaluso, and J. Y. Chan, Phys. Rev. Lett. **96**, 087204 (2006).
[14] Y. Machida, S. Nakatsuji, Y. Maeno, T. Tayama, T. Sakakibara, and S. Onoda, Phys. Rev. Lett. **98**, 057203 (2007).
[15] H. D. Zhou, C. R. Wiebe, J. A. Janik, L. Balicas, Y. J. Yo, Y. Qiu, J. R. D. Copley, and J. S. Gardner, Phys. Rev. Lett. **101**, 227204 (2008).
[16] Y. Machida, S. Nakatsuji, S. Onoda, T. Tayama, and T. Sakakibara, Nature (London) **463**, 210 (2009).
[17] M. Udagawa and R. Moessner, Phys. Rev. Lett. **111**, 036602 (2013).
[18] E.-G. Moon, C. Xu, Y. B. Kim, and L. Balents, Phys. Rev. Lett. **111**, 206401 (2013).
[19] R. Flint and T. Senthil, Phys. Rev. B **87**, 125147 (2013).
[20] G. Chen and M. Hermele, Phys. Rev. B **86**, 235129 (2012).
[21] S. Lee, A. Paramekanti, and Y. B. Kim, Phys. Rev. Lett. **111**, 196601 (2013).
[22] B. Kim, H. Jin, S. Moon, J.-Y. Kim, B.-G. Park, C. Leem, J. Yu, T. Noh, C. Kim, S.-J. Oh *et al.*, Phys. Rev. Lett. **101**, 076402 (2008).
[23] M. Kurita, Y. Yamaji, and M. Imada, J. Phys. Soc. Jpn. **80**, 044708 (2011).
[24] W. Witczak-Krempa, A. Go, and Y. B. Kim, Phys. Rev. B **87**, 155101 (2013).
[25] Y. Machida, S. Nakatsuji, H. Tonomura, T. Tayama, T. Sakakibara, J. Van Duijn, C. Broholm, and Y. Maeno, J. Phys. Chem. Solids **66**, 1435 (2005).
[26] S. Onoda and Y. Tanaka, Phys. Rev. Lett. **105**, 047201 (2010).
[27] The degeneracy of the non-Kramers doublet could be lifted, in principle, by a Jahn-Teller distortion of the surrounding oxygens. This would give rise to to on-site terms such as $Q^*\tau^+ + Q\tau^-$. Due to the lack of evidence for any significant splitting from experiments, we ignore this term.
[28] S. Onoda and Y. Tanaka, Phys. Rev. B **83**, 094411 (2011).
[29] S. B. Lee, S. Onoda, and L. Balents, Phys. Rev. B **86**, 104412 (2012).
[30] C. J. Bradley and A. P. Cracknell, *The Mathematical Theory of Symmetry in Solids: Representation Theory for Point Groups and Space Groups* (Clarendon Press, Oxford, 1972).
[31] P. Chandra, P. Coleman, and R. Flint, Nature (London) **493**, 621 (2013).
[32] J. H. Kim and J. H. Han, Phys. Rev. B **78**, 180410 (2008).
[33] F. J. Burnell, S. Chakravarty, and S. L. Sondhi, Phys. Rev. B **79**, 144432 (2009).
[34] X.-G. Wen, Phys. Rev. B **65**, 165113 (2002).
[35] P. Coleman, in *Handbook of Magnetism and Advanced Magnetic Materials*, edited by H. Kronmueller and S. Parkin (John Wiley & Sons, Hoboken, New Jersey, 2007).
[36] P. Coleman, J. B. Marston, and A. J. Schofield, Phys. Rev. B **72**, 245111 (2005).